ADVANCES IN FOOD AND NUTRITION RESEARCH, VOL. 40

Chapter 16

MODELING MEMBRANE TRANSPORT

RICHARD B. KING

Center for Bioengineering
University of Washington
Seattle, Washington 98195

I. INTRODUCTION

As research penetrates deeper and deeper into biological systems, we recognize increasing levels of complexity. This complexity arises from many sources, including the anatomy of the system, biochemical reactions within the tissue, feedback–control loops, and the presence of specialized transport mechanisms for specific substrates. The complexity present in the system often quickly exceeds our ability to intuitively predict its behavior, and

artificial aids to understanding become essential. A mathematical model[1] of the system that can be evaluated by a digital computer is one such aid.

The development of a mathematical model begins with an hypothesis that describes the system. The hypothesis is usually expressed as a set of differential equations that can be solved by a computer program. The computer implementation of the model provides not only a description of the system, but also predicts the response of the system to changing conditions. These predictions can be compared to real-world behavior. Since it will always be the case that the model is less complex than the real system, our comparisons will most often lead us to refine the model by increasing its complexity. The principles of formulating and testing mathematical models have been described by Berman (1963).

The design of a model is a compromise between attempting to describe the whole complexity of a real system and our ability to accurately deal with that complexity in the model. One approach to dealing with complexity is to begin with a set of submodels that are described as differential operators that take one or more inputs and operate on them to produce one or more outputs. These operators can then be connected together to produce more complex models.

When modeling passage of substrates across membranes, the simplest system is composed of two well-stirred compartments separated by a semipermeable membrane. This simple model is easy to describe mathematically and to implement on a computer. It is also, of course, unrealistically simple. First, the assumption of complete mixing is nearly always violated. When convection is involved, transport is a distributed process. That is, a concentration gradient exists along the axis of convection (e.g., from the proximal to the distal end of the intestine, from the arterial to the venous end of a capillary). Second, substrates traverse multiple membranes when passing from the lumen of the gut to the blood and from the blood to tissue. Finally, in many instances, there are specific transport mechanisms that move substrates across the membrane.

When a substrate must traverse a layer of cells to reach its target, the substrate molecules may move through gaps between the cells or they may move though the cell membrane. In the latter case, the substrate may move by pinocytosis, by "dissolving" in the membrane, or there may be a carrier-mediated transport mechanism for that substrate. Passage by dissolving in the membrane and passage through intercellular gaps may both be modeled as traversal of a semipermeable membrane, because the gaps present a passive diffusional barrier. Even when substrates move across membranes by passive diffusion, these membranes can have important effects on the

[1] Models used here are available from the author who can be contacted by electronic mail at rick@nsr.bioeng.washington.edu.

dynamic response of the system since the resistance to diffusion can introduce significant delays.

Carrier-mediated transport across membranes adds additional complexity to the system and, thus, to the model. For even the simplest transporter, the concentration of the transporter and its affinity for the substrate must be known before it can be modeled. Also, active transport is inherently a saturable process. Thus, to analyze the dynamics of tracer-labeled substrate, the model must account for both labeled and unlabeled substrate as the transport dynamics will depend on total substrate concentration.

II. A MULTIREGION, DISTRIBUTED EXCHANGE MODEL

A. MODEL STRUCTURE

A model for transport and exchange of tracer between plasma, endothelial cells, interstitial fluid, mucosal cells, and the lumen of the intestine is diagrammed in Fig. 1 for a single capillary–tissue unit. The model accounts for convection of tracer in the plasma (F_p) and in the lumen of the intestine (F_i). Material diffuses from region to region by conductance (PS) across the cellular membranes and through the gaps between the endothelial cells (PS_g). Each of the regions is characterized by the volume of distribution

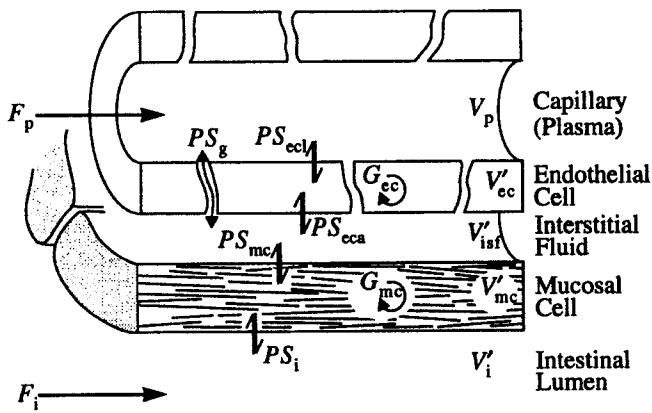

FIG. 1. Schematic representation of a five-region, axially distributed blood–tissue exchange model composed of plasma (p), endothelial cells (ec), interstitial fluid space (isf), mucosal cells (mc), and the intestinal lumen (i). Convection (F) takes place in both the plasma and intestinal lumen. The Vs are volumes of distribution. Barrier conductances are given by permeability–surface area products (PS). Reactions or metabolic consumption within the cells are given by the clearances (G).

(V') of the tracer being modeled. This volume may be smaller than the physical volume of the region if the tracer is excluded from some portion of the volume (e.g., exclusion from mitochondria in the cells) or larger in the presence of a mechanism that sequesters or concentrates the tracer. The model accounts for first-order consumption of tracer in the endothelial and mucosal cells (G). This model extends the four-region model described by Bassingthwaighte *et al.* (1989a) by including a fifth region, the intestine, with its flow.

The model is axially distributed which permits the development of concentration gradients in the axial direction in each of the regions. This is accomplished by dividing the capillary–tissue unit into a number of axial segments (N_{seg}). The number of segments used is under the control of the modeler. The actual length of the capillary–tissue unit need not be known unless axial diffusion is included (see Model Assumptions).

B. MODEL ASSUMPTIONS

The explicit model assumptions are:

1. The system is linear and stationary. Flows are constant and coefficients are not concentration dependent. *PS*s will be nonlinear for carrier-mediated transport, but are linear for tracers present in extremely low molar concentrations (Bassingthwaighte and Goresky, 1984).
2. The transport parameters are uniform in the axial direction. Deviations from this assumption have very little effect on outflow dilution curves but the effect on intratissue concentration profiles is large (Bassingthwaighte, 1974).
3. Convection occurs only in the capillary and lumen of the intestine.
4. There is no capacitance for solute in the membranes.
5. The outer boundaries are reflecting. This means there is no exchange between neighboring capillary–tissue units. The model is inappropriate for highly diffusible tracers such as gasses and heat because of diffusional shunting (Roth and Feigl, 1981; Sharan *et al.*, 1989).
6. Diffusion is rapid in the radial direction in all regions. This assumption seems to be valid for small solutes in well-perfused organs such as the heart (Bassingthwaighte and Goresky, 1984) and liver (Goresky, 1963), but may be violated in some tissues.
7. There is no diffusion in the axial direction. This assumption may be violated when molecular diffusion is fast compared to convection. Bassingthwaighte *et al.* (1992) present methods for incorporating axial diffusion into the model.

C. METHODS OF SOLUTION

1. Flow Algorithm

The flow through the capillary and intestine can be modeled in a number of ways. In their distributed blood–tissue exchange models, Bassingthwaighte *et al.* (1989a, 1992) have used the LaGrangian, or sliding element, algorithm which is illustrated on the left in Fig. 2. This assumes plug flow with a flat velocity profile in the flowing region. This algorithm allows for fast computation and introduces no dispersion. It does, however, give the model an inherent time step, which is the time required to fill one segment of the capillary, equal to $V_p/(F_p \cdot N_{seg})$.

With two flowing regions having different flows, the sliding element algorithm cannot be used. Instead a Poisson algorithm, illustrated on the right in Fig. 2, is used. This algorithm models the flowing region as a series of well-stirred tanks. At each time step, each segment of the flowing region loses some of its contents to the downstream segment and receives some of the contents of the upstream segment. If the time step is greater than

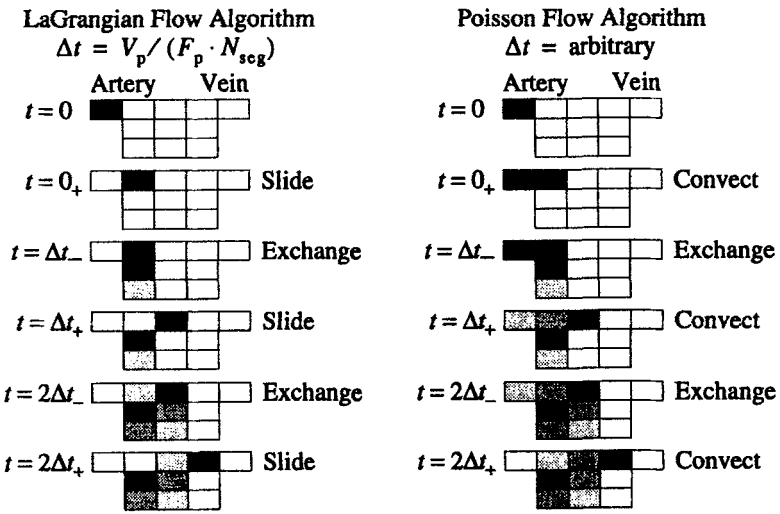

FIG. 2. Two algorithms for modeling flow. (Left) LaGrangian sliding fluid element algorithm. With each Δt the entire capillary contents slide one element downstream instantaneously. The slide is followed by transmembrane exchanges. (Right) Poisson-stirred tanks algorithm. At each Δt a portion of the contents of each capillary segment is transferred downstream. The convection is followed by transmembrane exchanges.

the time required to fill one segment of the flowing region, the algorithm is repeated until the convection is completed. This algorithm has the advantage of having no inherent time step. It does, however, introduce dispersion of the input function. The dispersion is minimized when the number of axial segments is large and when the input function is dispersed rather than a spike.

2. *Computation of Radial Exchanges*

The radial exchanges are calculated by an analytical solution to a linear set of ordinary differential equations describing the exchanges. The solutions for the concentrations in each region at time $t + \Delta t$ are

$$U(t + \Delta t) = e^{A\Delta t}U(t), \tag{1}$$

where U is the concentration vector. The term $e^{A\Delta t}$ can be computed analytically using an eigenvalue and eigenvector approach. Since the model is linear and stationary, $e^{A\Delta t}$ can be calculated once when the model is initialized and applied each time the model is evaluated.

The numerical methods for computing exchanges are described in detail in Bassingthwaighte *et al.* (1989a,b, 1992).

III. PASSIVE DIFFUSION

A. FLOW-LIMITED AND BARRIER-LIMITED EXCHANGE

When solutes passively diffuse across barriers such as the cell membranes or the gaps between endothelial cells, the presence of the diffusion barrier may significantly alter the behavior of the solute. The magnitude of this effect depends on the relative importance of diffusion compared to convection, which may be evaluated by the ratio of barrier conductance to flow (PS/F). This is illustrated in Fig. 3, which shows the behavior of an extracellular tracer, i.e., one which only permeates the endothelial cell gaps. In Figs. 3a and 3b the gap permeability, PS_g, is 100 ml g^{-1} min^{-1}. Figure 3a shows the outflow curves for three different plasma flows, 0.2, 1.0, and 2.0 ml g^{-1} min^{-1} (PS/F = 500, 100, and 50, respectively). With increasing flow, the peak of the curve shifts to the left, and mean transit time ($\bar{t}$ = F/V) decreases. Figure 3b shows these same curves scaled by their mean transit times. (The time axis is divided by $\bar{t}$ and the ordinate is multiplied by $\bar{t}$, thus preserving area.) The three scaled curves superimpose because

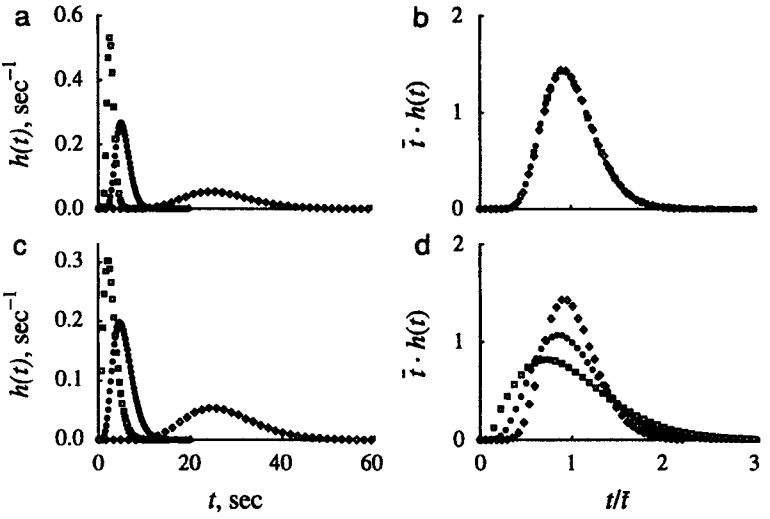

FIG. 3. Flow-limited and barrier-limited exchange. Outflow curves for an extracellular tracer with plasma flows of 0.2 (diamonds), 1.0 (circles), and 2.0 (squares) ml g^{-1} min^{-1}. (a) Flow-limited exchange with PS_g of 100 ml g^{-1} min^{-1}. (b) Curves from (a) scaled by their mean transit times, $\bar{t}$, showing similarity scaling. (c) Barrier-limited exchange with PS_g of 10 ml g^{-1} min^{-1}. (d) Transit time scaled curves from (c).

the transport from inflow to outflow is totally dominated flow and is not influenced, i.e., impeded, by the barrier.

In contrast, Figs. 3c and 3d show the behavior of the same tracer when PS_g is 10 ml g^{-1} min^{-1} (PS/F equal to 50, 10, and 5). While the shapes of the outflow curves do not appear much different, the scaled curves no longer superimpose. Their shapes are affected by the presence of the barrier which impedes the movement of tracer out of the plasma to the extracellular fluid and its backflux into the plasma.

B. TRACER WASHOUT

The rate at which solute is washed out of the capillary–tissue unit depends on the number of barriers that it must cross to reach a region in which it can be removed by convection. The washout rate is also affected by the volumes of the regions through which it is transported. Figure 4a shows the washout of tracer when the cells or the intestine are preloaded with tracer. In each case the plasma flow and all barrier conductances are 1 ml g^{-1} min^{-1}. (For simplicity, intestinal flow is set to zero.)

Tracer preloaded in the endothelial cells washes out rapidly because

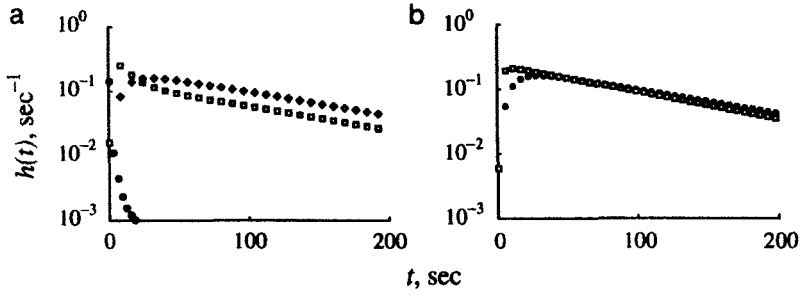

FIG. 4. Tracer washout after cell loading. Plasma outflow curves after: (a) loading in endothelium (circles), mucosa (squares), and intestine (diamonds) and (b) loading in the intestine with PS_i of 1 (circles) and 100 (squares). F_p = 1.0 ml g^{-1} min^{-1}, F_i = 0.0 ml g^{-1} min^{-1}, PS_{all} = 1.0 ml g^{-1} min^{-1}, V_p = 0.015 ml g^{-1}, V'_{ec} = 0.005 ml g^{-1}, V'_{isf} = 0.075 ml g^{-1}, V'_{mc} = 0.3 ml g^{-1}, V'_i = 0.4 ml g^{-1}.

the endothelial cell volume is small (0.005 ml g^{-1}), and the tracer only has to cross one barrier to reach the plasma. The washout curve is not monoexponential because some of the tracer diffuses across the abluminal surface of the endothelial cells into the interstitial fluid, mucosal cells, and intestinal lumen before diffusing back across the barriers into the plasma. Tracer preloaded into the mucosal cells and intestinal lumen washes out much more slowly since the volumes of these regions are large (0.3 and 0.4 ml g^{-1}, respectively) and it must traverse multiple barriers. The curve for preloading in the mucosa rises more rapidly, but at long times the washout rates are nearly identical.

A large change in the conductance of the luminal mucosal cell membrane, PS_i, has only a modest effect on tracer washout of tracer preloaded into the intestinal lumen, Fig. 4b. The curve rises more rapidly, but the washout rate is only slightly greater when the conductance is raised 100-fold.

Figure 5 shows tracer washout when a constant infusion of tracer is made into the plasma (Fig. 5a) or intestinal lumen (Fig. 5b). Flow through the intestinal lumen is 0.05 ml g^{-1} min^{-1}; membrane conductances, volumes, and plasma flow are identical to those used for Fig. 4a. The concentration of tracer in the plasma outflow rises more quickly in either case due to its much greater flow. The much higher plasma flow (20-fold greater than intestinal flow) results in nearly equal steady-state concentrations when the tracer is injected into the plasma and in a lower concentration in the plasma than in the intestine when the tracer enters through the intestine.

The flow difference explains the time required for the intestinal concentration to reach steady state. Tracer in the plasma is quickly convected to

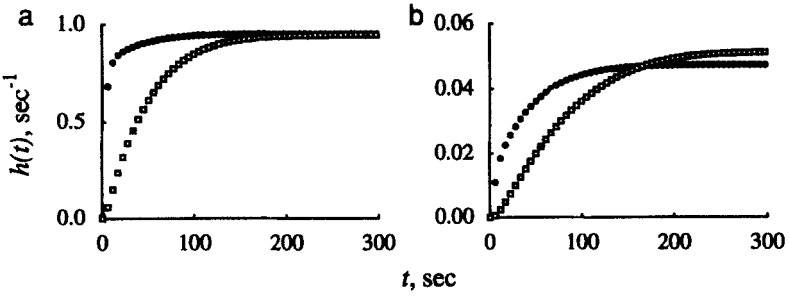

FIG. 5. Tracer washout curves with constant infusion of tracer. Plasma (circles) and intestine (squares) outflow curves with infusion into: (a) plasma and (b) lumen of the intestine. F_p = 1.0 ml g^{-1} min^{-1}, F_i = 0.05 ml g^{-1} min^{-1}, PS_{all} = 1.0 ml g^{-1} min^{-1}, V_p = 0.015 ml g^{-1}, V'_{ec} = 0.005 ml g^{-1}, V'_{isf} = 0.075 ml g^{-1}, V'_{mc} = 0.3 ml g^{-1}, V'_i = 0.4 ml g^{-1}.

the downstream end of the capillary where it can diffuse into the intestine. This "carriage effect" is much greater with plasma than with intestinal injection.

IV. CARRIER-MEDIATED TRANSPORT

A. INTRODUCTION

The introduction of carrier-mediated transport requires a redefinition of the model because it represents a partial relaxation of the first model assumption. When transport is carrier-mediated, the membrane transport parameters are concentration dependent and depend on the concentration of substrate on both sides of the membrane. The effect is to modify the conductance of the membrane, a fact that we will use in redesigning the model.

Carrier-mediated transport is a saturable process. The carrier has a finite concentration in the membrane. When the concentration of the substrate is high enough, all the carrier will be bound to the substrate and adding additional substrate will not result in increased transport. When a tracer is used, the carrier will exhibit competitive inhibition. Labeled substrate must compete with unlabeled substrate for available carrier. Thus, increased concentrations of unlabeled substrate may result in decreased transport of tracer. To account for this, the model must account for both tracer and mother (nontracer) substances.

B. ONE-SITE, TWO-SIDED TRANSPORTER MODEL

1. *Transporter Configuration*

A simple one-site, two-sided transporter is diagrammed in Fig. 6. The transporter, T, can reversibly bind with the substrate, C, on either side of the membrane. The equilibrium dissociation constants, D_i and D_o, are the ratio of the reaction rate for the dissociation reaction to that for the association reaction (off-rate to on-rate) on the inside and outside surfaces of the membrane, respectively. The units of D are millimolar (mM, or whatever units are being used for concentration).

Both the free transporter and the transporter–substrate complex, TC, can diffuse through the membrane. P_0 and P_1 are the permeabilities of the free transporter and complexed transporter, respectively. The units of P are per minute.

2. *Calculating Membrane Conductances*

A concentration-dependent expression for membrane conductance can be derived by starting with Ohm's law.

$$\text{Current} = \text{Driving Force} \cdot \text{Conductance}. \tag{2}$$

In our case, current is the flux of substrate across the membrane (J), driving force is the concentration of the substrate (C), conductance is the membrane conductance (PS), and Eq. (2) can be rewritten as

$$PS = \frac{J}{C}. \tag{3}$$

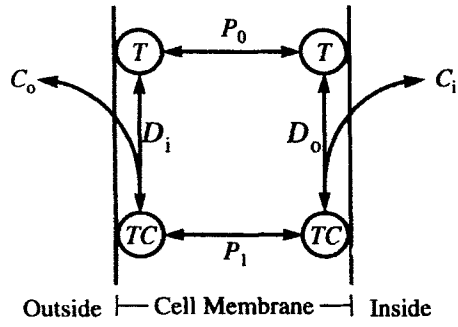

$$T + C \underset{\alpha}{\overset{a}{\rightleftharpoons}} TC$$

$$D_i = \frac{\alpha_i}{a_i} = \frac{T_i \cdot C_i}{TC_i}$$

$$D_o = \frac{\alpha_o}{a_o} = \frac{T_o \cdot C_o}{TC_o}$$

FIG. 6. Diagram of a one-site, two-sided transporter model.

The flux from the *cis*- to the *trans*-side of the membrane is

$$J_{io} = \frac{C_T P_1 \gamma_o C_i}{D_i(\gamma_o \delta_i + \gamma_i \delta_o)}, \tag{4}$$

where C_T is the concentration of the transporter in the tissue, mM, and

$$\gamma_0 = P_0 + \frac{P_1 C_o}{D_o} \quad \gamma_i = P_0 + \frac{P_1 C_i}{D_i}$$
$$\delta_0 = 1 + \frac{C_o}{D_o} \quad \delta_i = 1 + \frac{C_i}{D_i}.$$

Note that in Eq. (4) the subscripts *i* and *o* refer to the *cis*- and *trans*-sides of the membrane, respectively, rather than the inside and outside of the cell.

From Eqs. (3) and (4), we can write expressions for the conductance of the outside and inside surfaces of the membrane in terms of the substrate concentrations, dissociation constants, transporter permeabilities, and concentration of transporter in the tissue.

$$PS_i = \frac{C_T P_1 \left(P_0 + \frac{P_1 C_i}{D_i}\right)}{D_o\left[\left(1 + \frac{C_o}{D_o}\right)\left(P_0 + \frac{P_1 C_i}{D_i}\right) + \left(1 + \frac{C_i}{D_i}\right)\left(P_0 + \frac{P_1 C_o}{D_o}\right)\right]}, \text{ and} \tag{5}$$

$$PS_o = \frac{C_T P_1 \left(P_0 + \frac{P_1 C_o}{D_o}\right)}{D_i\left[\left(1 + \frac{C_o}{D_o}\right)\left(P_0 + \frac{P_1 C_i}{D_i}\right) + \left(1 + \frac{C_i}{D_i}\right)\left(P_0 + \frac{P_1 C_o}{D_o}\right)\right]}, \tag{6}$$

where PS_i is the conductance from the outside to the inside of the cell and PS_o is the conductance from inside to outside.

Figure 7 shows the conductance of a membrane with the one-site carrier with changing concentration of substrate on the outside, C_o, and inside, C_i, of the membrane. As C_o increases, more of the carrier is bound to the substrate, less is available to bind more substrate, and the membrane conductance decreases. Similarly, increases in C_i decrease the conductance. When C_i is 5 mM, nearly all the carrier is bound to substrate on the inside of the membrane and conductance is reduced to near zero regardless of the outside concentration. Figure 7b illustrates asymmetric transport. The dissociation constant on the outside of the membrane is three times that on the inside, and the outward conductance is three times the inward

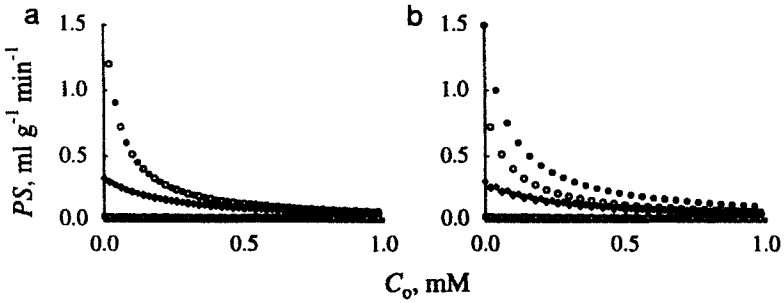

FIG. 7. Effective membrane *PS* in the inward (open symbols) and outward (filled symbols) directions as a function of substrate concentration on the outside of the membrane for inside concentrations (C_i) of 0.02 (circles), 0.2 (diamonds), and 2.0 (squares) m*M*. (a) Symmetric ($D_o = D_i$) and (b) asymmetric transport ($D_o = 3D_i$). $P_0 = P_1 = 6 \times 10^{-3}$ sec^{-1}, $D_o = 10^{-2}$ m*M*, $C_T = 0.2$ m*M*

conductance. Changes in P_0 relative to P_1 will not produce asymmetric transport, but will alter the conductances in both directions.

3. *A Blood–Tissue Exchange Model with Carrier-Mediated Transport*

The model shown in Fig. 1 can be modified to include the carrier-mediated transport. Figure 8 shows such a model with carriers on the membranes of

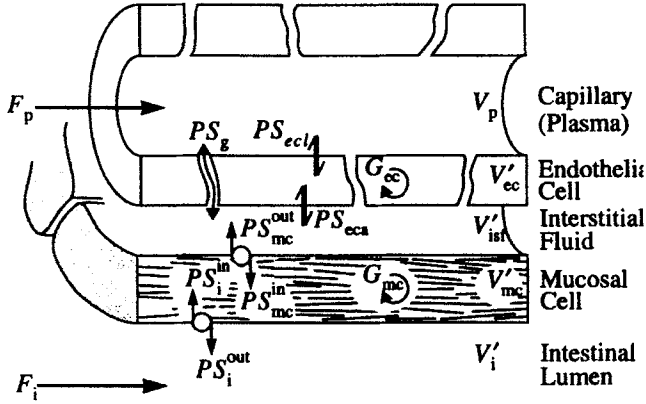

FIG. 8. Schematic representation of a five-region, axially distributed blood–tissue exchange model with carrier-mediated transport on the membranes of the mucosal cell. See the legend to Fig. 1 for an explanation of symbols.

the mucosal cells. This requires three changes in the implementation of the model. First, the model must account for tracer and nontracer substrate. Second, the effective conductances of the mucosal cell membranes are calculated from the substrate concentrations and the parameters of the transporter. Since the conductances are dependent on concentrations that change with time and axial position in the capillary–tissue unit, the third change is to calculate the coefficients of the updating matrix, $e^{A\Delta t}$ of Eq. (1), for each axial segment each time the model is evaluated. This has a impact on model performance since the calculations required to evaluate the updating matrix are costly.

C. TRACER STUDIES

Figure 9 shows a simulation experiment examining the behavior of the carrier-mediated transport model following a constant infusion of tracer into the lumen of the intestine. The total substrate concentration was constant at 10^{-2} mM and the tracer concentration was 10^{-8} mM throughout the experiment. Figure 9a shows the concentration of tracer in the outflow of the plasma and intestine. (Note the ordinate has a logarithmic scale.) The final concentration in the intestinal outflow is 0.9×10^{-8} mM. Most of the tracer is passing through the intestine without being absorbed through

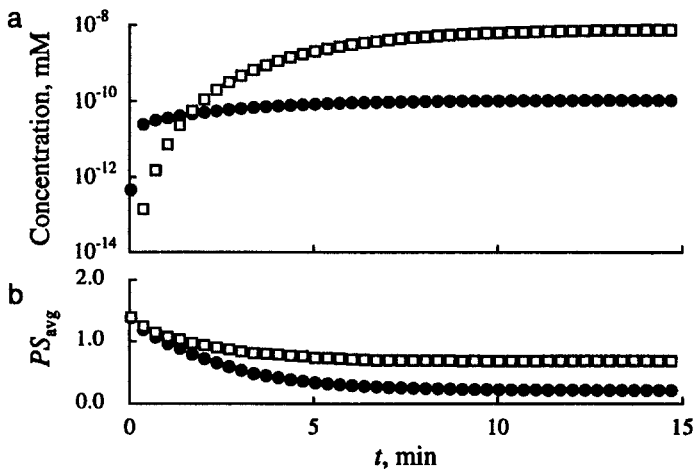

FIG. 7. Outflow concentration (a) for plasma (circles) and intestine (squares) and average membrane conductance (b) for the intestine–mucosal cell (circles) and mucosal cell–isf (squares) exchange following constant infusion of substrate and tracer into the inflow to the intestinal lumen at a total substrate concentration of 10^{-2} mM. See the legends to Figs. 5 and 7 for the values of the parameters for flows and volumes and of the transporter.

the mucosa. In this experiment, the equilibrium dissociation constant on the outside of the membrane is 10^{-6} mM. Thus the total substrate concentration at the inflow is 10^4 times the dissociation constant, causing most of the carrier to be bound on the outside surface of the membrane and not be available for transport. This is also apparent from Fig. 9b, in which the average membrane conductance is plotted as a function of time. The average is obtained from the arithmetic mean of the conductances in each axial segment; since D_i equals D_o, the transport is symmetric and PS^{out} equals PS^{in}. The PS_i has an initial value of 1.4 ml g^{-1} min^{-1} but falls to a steady-state value of only 0.2. The steady-state value of PS_{mc} is higher, 0.7 ml g^{-1} min^{-1}, because it sees a much lower substrate concentration.

The steady-state plasma outflow concentration, 2.6×10^{-11} mM, is much lower than that for the gut. This is explained by the low membrane permeabilities and by the much higher flow rate of the plasma (20-fold greater than that in the intestine). Note that this steady-state concentration is more than two orders of magnitude less than that in the intestine. This contrasts markedly with the relatively small difference seen when membrane conductances are not sensitive to substrate concentration, Fig. 5b.

Figure 10 shows the effect on tracer extraction from the gut with constant infusion of substrate at different concentrations. Extraction measures the amount of tracer that is absorbed in a single pass through the gut. In the steady state, the extraction, $E(t)$, is defined as

$$E(t) = 1 - \frac{C_{out}(t)}{C_{in}(t)}. \tag{7}$$

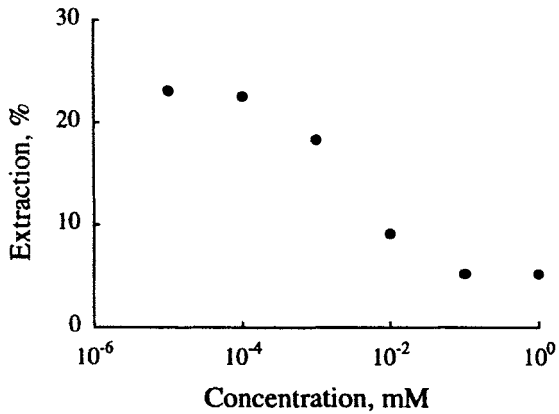

FIG. 10. Extraction of tracer from the gut as a function of total concentration of the substrate. See the legend to Fig. 9 for experimental details.

At very low substrate concentrations, the maximum extraction is 23%. As substrate concentration increases, extraction declines to 9% at the substrate concentration of 10^{-2} mM used in Fig. 9 and reaches a minimum of about 5% at 0.1 mM. In the real world, the extraction would continue to decline until extraction was essentially zero and all carrier was bound. The plateau at 5% is an artifact of the numerical methods used by the model to keep the solution stable.

D. OTHER CARRIER MODELS

The single-site model used thus far is the simplest carrier model. Many other configurations are possible and probably exist in the body. Two examples are diagrammed in Fig. 11. The two-site carrier is a simplification of the carrier proposed for Ca–Na exchange by Wong and Bassingthwaighte (1981). A detailed discussion of different types of carriers and their dynamics is given by Stein (1986). Regardless of the carrier model used, a strategy for incorporating it into a model is to derive the equation for unidirectional flux, and then use that result to get the effective membrane conductance.

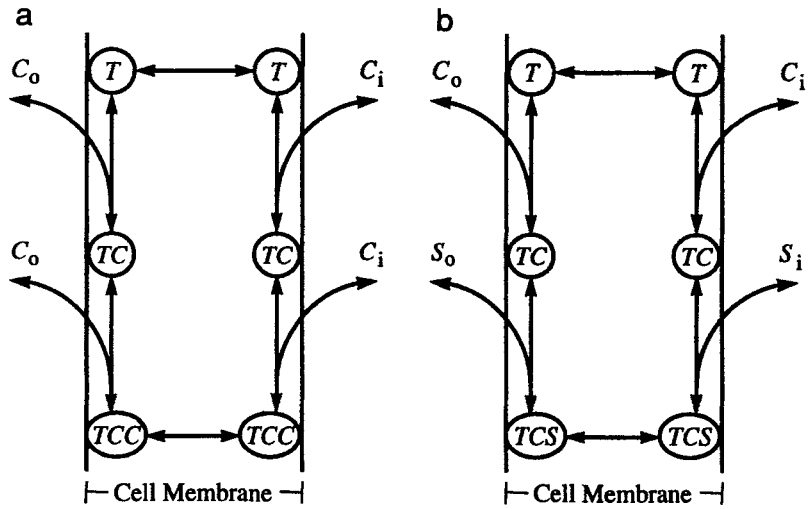

FIG. 11. Diagram of two carrier models. (a) Two-site carrier model. The carrier (T) has two active sites that bind the same substrate (C). Only the uncomplexed and doubly complexed forms of the carrier can move across the membrane. (b) Cotransporter. Similar to (a) but the one active site of the transporter binds the first substrate (C) but the second site binds a second substrate (S).

V. BUILDING COMPLEX MODELS

A. INTRODUCTION

The illustrations above all use a single capillary model in an open (nonrecirculating) system. While the latter is not a limitation if the input and output concentration–time curves can be measured across the region or organ of interest, single capillary models are seldom appropriate for modeling a whole organ as this makes the assumption that the organ is internally homogeneous. Even considering the flow only, this assumption is invalid (King *et al.*, 1985, for example), and heterogeneities also exist in other quantities such as metabolism, oxygenation, and, most likely, local membrane conductance. For many investigations, therefore, it is necessary to assemble models of whole organs or organ systems, and, for some, a model of the whole body is required.

B. DIFFERENTIAL OPERATORS

One approach to the design of complex models is to build differential operators that can be assembled into a complete model in a hierarchical manner. A differential operator can be simply defined as an operator that takes one or more inputs and manipulates them in some way to produce one or more output responses continuously. (In a computer model, a differential operator becomes a function, subroutine, or procedure.)

The approach is illustrated in Fig. 12 for the construction of a vascular operator that can be used to model transport through a nonexchanging

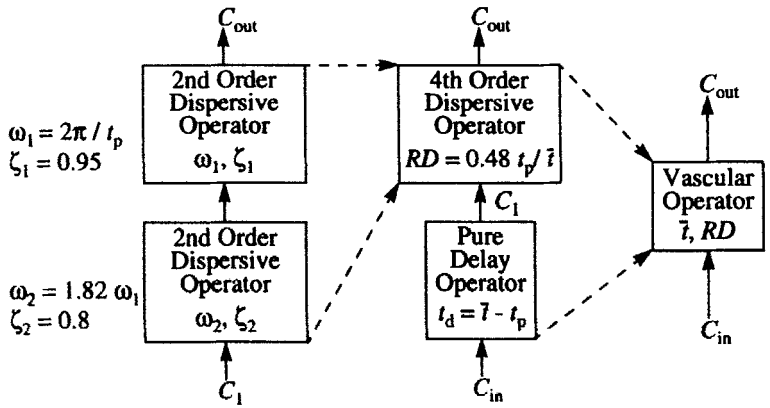

FIG. 12. Construction of a differential operator for vascular transport from simpler differential operators.

vessel (King *et al.*, 1993). The operator is composed of two simpler operators, a pure delay operator and a second-order dispersive operator that provides an analytic solution to the equation

$$\frac{d^2C}{dt^2} + 2\omega\zeta\frac{dC}{dt} + \omega^2C = \omega^2 f, \tag{8}$$

where C is the output concentration, f is the input concentration, ω is the natural frequency in radians per second, and ζ is the dimensionless damping coefficient. Two second-order operators are connected together to make a fourth-order dispersive operator which is connected to a delay operator to form the completed vascular operator. From the parameters of the vascular operator, transit time ($\bar{t}$) and relative dispersion (RD), the parameters of each of the simple operators can be calculated. (The differential operators are usually implemented as reentrant computer code so that only a single copy is required in a model.)

C. ORGAN MODELS

Differential operators can be used to build organ models. Figure 13 shows two different styles of organ models. Figure 13a shows a parallel pathway model that might be appropriate for an organ like the heart. The exchange unit in each pathway could be a distributed capillary–tissue exchange operator. The artery, arterioles, venules, and vein can be modeled by the vascular operator shown in Fig. 12. The transport parameters of each pathway can be independent to model heterogeneity in the organ.

Figure 13b depicts a serial arrangement that could be appropriate for the intestine. Here the exchange units are dual flow operators like those illustrated in Fig. 8. For this model, it would be useful to make a new operator composed of an artery, vein, and exchange unit; these operators could then be linked serially to create the whole organ model.

D. WHOLE-BODY MODELS

The use of differential operators facilitates the construction of whole-body models. The operators can easily be interconnected in the arrangement required for a complex closed-loop system, and the use of a hierarchical structure makes the model structure clearly visible at each level.

Creating a whole-body model for a given substrate depends on having a toolkit of operators that are appropriate for the substrate. Considerable care should be taken in the design of the toolkit and in the numerical methods used. Effort spent in this design will be repaid when the compre-

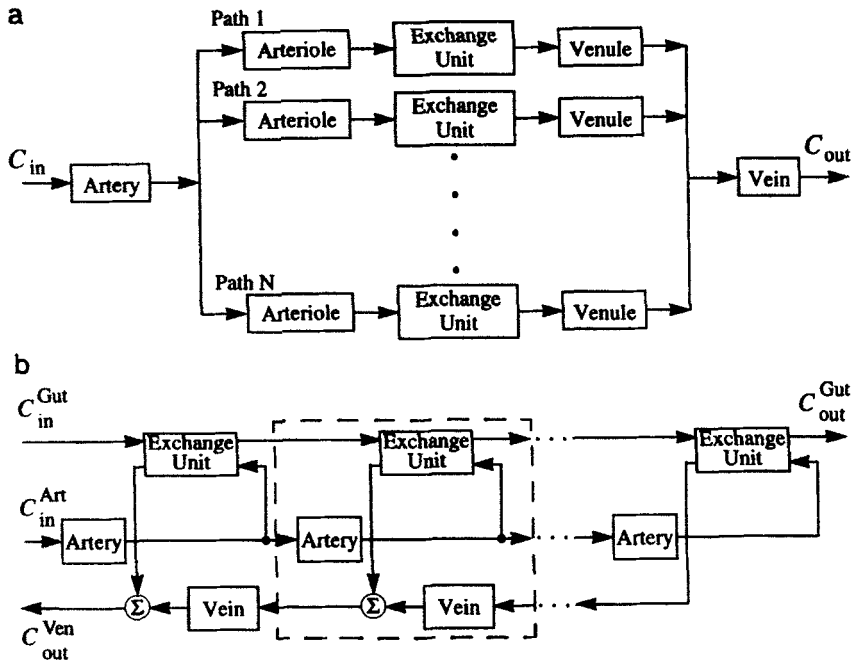

FIG. 13. Two different styles of organ models composed of simpler differential operators. (a) A parallel pathway model fed by a single artery and drained by a single vein. Each pathway has a capillary–tissue exchange unit fed by an arteriole and drained by a venule. (b) A dual flow organ with operators connected in series. The dashed line shows the basic unit of the organ composed of arterial, venous, and capillary–tissue exchange unit operators.

hensive model can be assembled with ease and produces stable, accurate results. The complexity required of the model depends, of course, on the substance being investigated. King *et al.* (1993) show a simple whole-body model for an intravascular tracer that is constructed using only the vascular operator shown in Fig. 12.

VI. SUMMARY

Many substrates cross cell membranes by processes other than passive diffusion. When the transport is carrier-mediated, e.g., facilitated diffusion, active transport, and exchange diffusion, the carrier modifies the conductance of the membrane and may either increase or decrease the flux of the substrate across the membrane. A common characteristic of all carrier-

mediated transport is its saturability, as only a finite amount of carrier is available to bind with the substrate; even the simplest one-site carrier model exhibits saturation. Inclusion of carrier-mediated transport adds additional model parameters that describe the transporter. In addition, the model must account for both labeled (tracer) and unlabeled (mother) substrate, but this introduces no new parameters.

There are many possible models for a membrane carrier. The applicability of these models must be examined for the specific substrate of interest. Many experiments aimed at measuring carrier parameters are carried out on isolated cells or cell fragments. Experiments in intact organs (either *in vivo* and *in vitro*) are also possible. Of particular note is the "bolus sweep" method described by Rickaby *et al.* (1981) and Malcorps *et al.* (1984).

The increasing sophistication of experimental procedures, data collection techniques, and computers available to investigators continues to extend the depth to which we can probe biological systems. With this increased sophistication comes increased costs in time and equipment. It behooves us then to extract the maximum amount of information from each experimental procedure. Mathematical models assist in doing so, and sophistication in model analysis should parallel that in other phases of the experiment.

Increased realism brings several advantages. Simplification of a model to increase its ease of usage and speed in routine data analysis is a desirable goal, and comparing a simplified model against a more realistic model under the conditions specific to a given experiment is one way to test the simplifying assumptions. Additionally, increased model realism can bring new insight into unknown aspects of the system. All models, no matter how realistic, are always "wrong" in that they are less complex than the real system. Failure of the model to explain observed results forces us to further refine the model and teaches us something more about the system.

ACKNOWLEDGMENTS

This work is supported by NIH Grants RR-01243 and HL-19139.

REFERENCES

Bassingthwaighte, J. B. (1974). A concurrent flow model for extraction during transcapillary passage. *Circ. Res.* **35**, 483–503.

Bassingthwaighte, J. B., and Goresky, C. A. (1984). Modeling in the analysis of solute and water exchange in the microvasculature. *In* "Handbook of Physiology" (E. M. Renkin and C. C. Michel, eds.), Sect. 2, Vol. IV, pp. 549–626. Am. Physiol. Soc., Bethesda, MD.

Bassingthwaighte, J. B., Wang, C. Y., and Chan, I. S. (1989a). Blood-tissue exchange via transport and transformation by endothelial cells. *Circ. Res.* **65**, 997–1020.

Bassingthwaighte, J. B., Chan, I. S., and Wang, C. Y. (1989b)."Blood-tissue Exchange Models: BTEX30 and BTEX40(UW/BIOENG-89/1)," Report PB90-501396: FORTRAN Code; PB90-172578: Descriptive Text." Nat. Tech. Inf. Serv., Springfield, VA.

Bassingthwaighte, J. B., Chan, I. S., and Wang, C. Y. (1992). Computationally efficient algorithms for capillary convection-permeation-diffusion models for blood-tissue exchange. *Ann. Biomed. Eng.* **20,** 687–725.

Berman, M. (1963). The formulation and testing of models. *Ann. N.Y. Acad. Sci.* **108,** 182–194.

Goresky, C. A. (1963). A linear method for determining liver sinusoidal and extravascular volumes. *Am. J. Physiol.* **204,** 626–640.

King, R. B., Bassingthwaighte, J. B., Hales, J. R. S., and Rowell, L. B. (1985). Stability of heterogeneity of myocardial blood flow in normal awake baboons. *Circ. Res.* **57,** 285–295.

King, R. B., Deussen, A., Raymond, G. R., and Bassingthwaighte, J. B. (1993). A vascular transport operator. *Am. J. Physiol.* **265,** H2196–H2208.

Malcorps, C. M., Dawson, C. A., Linehan, J. H., Bronikowski, T. A., Rickaby, D. A., Herman, A. G., and Will, J. A. (1984). Lung serotonin uptake kinetics from indicator-dilution and constant-infusion methods. *J. Appl. Physiol.* **57,** 720–730.

Rickaby, D. A., Linehan, J. H., Bronikowski, T. A., and Dawson, C. A. (1981). Kinetics of serotonin uptake in the dog lung. *J. Appl. Physiol.* **51,** 405–414.

Roth, A. C., and Feigl, E. O. (1981). Diffusional shunting in the canine myocardium. *Circ. Res.* **48,** 470–480.

Sharan, M., Jones, M. D., Jr., Koehler, R. C., Traystman, R. J., and Popel, A. S. (1989). A compartmental model for oxygen transport in brain microcirculation. *Ann. Biomed. Eng.* **17,** 13–38.

Stein, W. D. (1986). "Transport and Diffusion across Cell Membranes." Academic Press, Orlando, FL.

Wong, A. Y. K., and Bassingthwaighte, J. B. (1981). The kinetics of Ca-Na exchange in excitable tissue. *Math. Biosci.* **52,** 275–310.